Polymer 49 (2008) 3533–3540

Contents lists available at ScienceDirect

Polymer

journal homepage: www.elsevier.com/locate/polymer

Viscoelastic and dielectric studies on comb- and brush-shaped poly(*n*-butyl acrylate)

Guy C. Berry [a,*], Stefan Kahle [b], Shigeki Ohno [a], Krzysztof Matyjaszewski [a], Tadeusz Pakula [b]

[a] Department of Chemistry, Carnegie Mellon University, 4400 Fifth Avenue, Pittsburgh, PA 15213, United States
[b] Max-Planck Institute for Polymer Research, D55021 Mainz, Germany

ARTICLE INFO

Article history:
Received 28 April 2008
Received in revised form 4 June 2008
Accepted 6 June 2008
Available online 17 June 2008

Keywords:
Brush-shaped polymer
Comb-branched polymer
Dynamic compliance

ABSTRACT

The dynamic compliances $J'(\omega)$ and $J''(\omega)$ and the dielectric permittivities $\varepsilon'(\omega)$ and $\varepsilon''(\omega)$ are reported over a wide range of frequency ω and temperature for comb-branched and brush-shaped poly(*n*-butyl acrylate) prepared by atom transfer radical polymerization. The analysis here of the viscosity η for the comb- and brush-shaped polymers indicates the need to account for an increase of the persistence length with increasing density of the side chains. Enhanced values of J_S are attributed to a dilution effect arising from the side chains on the values that would otherwise arise from the backbone chain. The dielectric loss $\varepsilon''(\omega)$ demonstrates a deviation from frequency–temperature superposition at a certain range of frequency, with the deviation increasing with increasing density of the side chains. The deviation occurs for a frequency range for which $J'(\omega)$ and $J''(\omega)$ are approaching their terminal response, but no corresponding deviation from frequency–temperature superposition is noted for these functions. The dielectric behavior in this region is attributed to a δ-relaxation at frequencies lower than the principal α-relaxation, similar to behavior reported for certain polymers with mesogenic side chains.

1. Introduction

This investigation will report frequency dependent linear viscoelastic compliance and dielectric permittivity of comb-shaped branched polymers based on poly(*n*-butyl acrylate), p*n*BuA, including densely branched brush polymers. A previous study on similar brush-shaped copolymers crosslinked either covalently or physically resulted in elastomers with an unusually low equilibrium shear modulus G_e, of order 1 kPa [1]. That behavior was attributed to the effect of the side chains on the brush polymers, which behave in some respect as a low molecular weight diluent that cannot be leached from the sample. Those samples were synthesized by controlled radical polymerization methods that grew the branches from functional groups on a pre-polymerized backbone chain. In this work, macromonomers based on poly*n*BuA were prepared by atom transfer polymerization, ATRP [2,3], to give chains of well-defined degree of polymerization. As described elsewhere [4], the macromonomers were either polymerized alone to give brush-shaped chain homopolymers or copolymerized with *n*-butyl acrylate to give comb-shaped polymers, using ATRP methods in either case.

The viscoelastic data reported here are presented as the dynamic compliances $J'(\omega)$ (in-phase component) and $J''(\omega)$ (out-of-phase component) determined over a wide range of temperature T and frequency ω on the bulk polymers. The corresponding dynamic dielectric functions $\varepsilon'(\omega)$ and $\varepsilon''(\omega)$ are reported as functions of ω and T. As discussed in the prior work, $J'(\omega)$ and $J''(\omega)$ may be represented by the expressions from linear viscoelasticity [5,6]:

$$J'(\omega) - J_g = \Delta J\left\{1 - \omega\int_0^\infty du\, r(u)\sin(\omega u)\right\} \tag{1}$$

$$J''(\omega) - 1/\omega\eta = \Delta J\omega\int_0^\infty du\, r(u)\cos(\omega u) \tag{2}$$

where $\Delta J = J'(0) - J_g$. In these expressions, $r(t)$ decreases monotonically from unity to zero with increasing t, most directly defined in terms of the creep compliance $J(t)$. For a fluid with viscosity η, (linear) recoverable compliance J_S and "instantaneous", or glassy, compliance J_g appearing in an expression for $J(t)$:

$$J(t) = J_g + \Delta J[1 - r(t)] + t/\eta \tag{3}$$

For the linear viscoelastic fluid, $J'(\omega)$ is equal to J_S and J_g and in the limits as ω goes to zero and infinity, respectively. In the prior work, it was found that the functions $J'(\omega)$ and $J''(\omega)$ displayed the so-called time–temperature superposition, whereby $J'(a_T\omega)/b_T$ and $J''(a_T\omega)/b_T$ could each be represented as superposed functions of $a_T\omega$

* Corresponding author. Tel.: +1 412 268 3131; fax: +1 412 268 6897.
E-mail address: gcberry@andrew.cmu.edu (G.C. Berry).

0032-3861/$ – see front matter © 2008 Elsevier Ltd. All rights reserved.
doi:10.1016/j.polymer.2008.06.015

at some reference temperature T_{ref}, where $b_T = [\Delta J(T)]/[\Delta J(T_{ref})]$ and $a_T = b_T\eta(T)/\eta(T_{ref})$ (in fact, b_T did not depend on T in the prior work). This superposition implies that the retardation function $r(t/a_T)$ defined in terms of a reduced time is independent of T over the time scale investigated. Analogous behavior will be observed with the data reported below.

Similarly, (aside from certain instrumental effects at small ω discussed below) the dynamic dielectric permittivity may be represented in the forms [7]

$$\varepsilon'(\omega) - \varepsilon_g = \Delta\varepsilon\left\{1 - \omega\int_0^\infty du\, e(u)\sin(\omega u)\right\} \quad (4)$$

$$\varepsilon''(\omega) - \sigma/\omega = \Delta\varepsilon\omega\int_0^\infty du\, e(u)\cos(\omega u) \quad (5)$$

where $\Delta\varepsilon = \varepsilon'(0) - \varepsilon_g$ and $e(t)$ is a dielectric retardation function that decrease monotonically from unity to zero with increasing t, $\Delta\varepsilon$ (>0) is the difference between the values of $\varepsilon'(\omega)$ as ω tends to zero or its value ε_g as ω approaches infinity, respectively, and σ is the d.c. conductivity σ^o divided by the dielectric permittivity of vacuum. It will be found that a reasonable time–temperature superposition obtains for $\varepsilon'(\omega)$ and $\varepsilon''(\omega)$ for the comb-shaped chain with relatively few, short branches, but that considerable deviation from this behavior obtains for $\varepsilon''(\omega)$ over a particular range of ω with increasing branch density. Unlike $r(t/a_T)$, the function $e(t/a_T)$ does not appear to be single-valued over the entire range of t and temperature, even though that behavior may be a reasonable approximation for some regimes of response, as discussed below. Comparison with similar deviations seen with certain polymers with liquid-crystalline side chains will be discussed below [8].

2. Experimental

2.1. Polymer synthesis

The four copolymers (series GP) and two of the homopolymers (series PMM) used in this study were prepared in the investigation described in Ref. [4]; the synthetic methods and the structural characterization are described therein. The two acryloyl-terminated poly(*n*-butyl acrylate) macromonomers (MM), A-(nBuA)$_x$, used were prepared by ATRP to yield a well-defined polymers p(A-(nBuA)$_x$) or copolymers p((A-(nBuA)$_x$)$_p$-*co*-(nBuA)$_y$) with poly(*n*-butyl acrylate), pnBuA, with a narrow molecular weight distribution, differing in their degree of polymerization. Since the reactivities of *n*-butyl acrylate and the macromonomer MM toward a growing pnBuA radical were found to be similar ($r_{n\mathrm{BuA}} \approx 1.10$), the distribution of the branches along the backbone of the comb-shaped GP series of polymers is essentially random [4]. The characterizing parameters given in Ref. [4] are presented in Table 1; x was determined by NMR end-group analysis and p and y were determined by analysis of the composition and conversion during polymerization. As may be seen in Table 1, three of the four copolymers have similar backbone degree of polymerization $DP_{n,bb} = y + p \approx 384$–$433$, with two of these sharing similar separation of branch points, $DP_{n,\Delta p} = y/p \approx 34$–$38$, but different branch $DP_{n,br} = x = 10$ for the branches (GP1 and GP5), and three sharing similar $DP_{n,br} = 42$, with two of these sharing similar $DP_{n,\Delta p} \approx 7$–$10$, but with different $DP_{n,bb}$ (GP3 and GP4). Two homopolymers were prepared with the lower DP macromonomer, one by ATRP methods (PMM2a), and the other using conventional free-radical polymerization (PMM2d). These were limited to a relatively low degree of polymerization ($DP_{bb} = p$), attributed to steric congestion restricting access of the macromonomer to the active chain end [4]. Finally, two high molecular weight brush-shaped homopolymers (HL2 and HL3) were prepared by the methods described previously [1]. The structures of the series GP and PMM polymers are contrasted with that of the series HL chains in Scheme 1 In the terminology of Ref. [4], these two polymers would be identified as p(BPEM$_p$-*g*-p(nBuA)$_x$), with x equal to the degree of polymerization of the BuA in the side chains, see Table 1.

Table 1
Polymeric structures studied

Series	$DP_{n,br}$[a]	p	y	$DP_{n,bb}$[b]	$DP_{n,\Delta p}$[c]	$DP_{n,tot}$[d]	λ[e]
GP5	25	10	423	433	38	683	0.63
GP1	42	10	374	384	34	804	0.48
GP3	42	35	353	388	10	1858	0.21
GP4	42	11	87	98	7	560	0.18
PMM2a	25	22	0	22	0	585	0.038
PMM2d	25	35	0	35	0	910	0.038
HL2	20	400	0	400	0	8400	0.048
HL3	40	400	0	400	0	16,400	0.024

Series GP and PMM: p((A-(nBuA)$_x$)$_p$-*co*-(nBuA)$_y$); series HL: p(BPEM$_p$-*g*-p(nBuA)$_x$).
[a] $DP_{n,br} = x$; the number-average degree of polymerization of *n*-BuA in a branch.
[b] $DP_{n,bb} = p + y$; the number-average number of repeat units in the backbone.
[c] $DP_{n,\Delta p} = y/(p+1)$; the number-average degree of polymerization of *n*-BuA between branches; $y > 0$ or $y = 0$ for comb-branched or brush chains, respectively.
[d] $DP_{n,tot} = DP_{bb} + pDP_{n,br}$; the total number-average degree of polymerization.
[e] $\lambda = DP_{bb}/DP_{n,tot}$; the fraction of the total mass in the backbone.

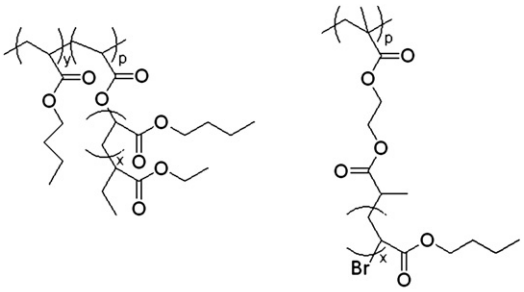

Series GP and PMM: p((A-(nBuA)$_x$)$_p$-*co*-(nBuA)$_y$)

Series HL: p(BPEM$_p$-*g*-p(nBuA)$_x$)

Scheme 1.

2.2. Mechanical properties

Dynamic mechanical measurements were carried out with the apparatus and methods described in Ref. [1]. Shear deformation was applied under condition of controlled deformation amplitude, always remaining in the range of the linear viscoelastic response of studied samples. The data, measured over the frequency range 0.1–100 rad/s at temperatures from −50 to 50 °C, are expressed as the dynamic storage and loss shear compliances, $J'(\omega)$ and $J''(\omega)$, respectively.

2.3. Dielectric properties

Isothermal frequency scans were performed in the temperature range from −60 to +100 °C. A Novocontrol BDS 4000 broad band dielectric spectrometer (based on a high resolution ALPHA Analyzer) was used to measure the dielectric function $\varepsilon^*(\omega) = \varepsilon'(\omega) - i\varepsilon''(\omega)$ at 10 points per frequency decade in the frequency range 10^{-1}–10^7 Hz. The sample capacitor consisted of two parallel gild brass-plates with a diameter of 20 mm, separated by the sample. A plate distance of 0.1 mm was kept constant by small Teflon™ spacers.

3. Results

3.1. Dynamic mechanical properties

The data on $J'(\omega)$ and $J''(\omega)$ as functions of ω and T were superposed as $J'(a_T\omega)$ and $J''(a_T\omega)$ as functions of $a_T\omega$ for a reference temperature $T_{ref} = 15\ ^\circ C$. Values of a_T were obtained to superpose the data on the assumption that b_T is independent of T, which is consistent with the data. An example of the reduced functions is given in Fig. 1 for data on GP5. Similar superposition was observed for all of the samples, with the results for a_T given in Fig. 2. As may be seen, essentially the same a_T were successfully used for all of the samples. The fundamental significance of this observation may be compromised by the relatively narrow (three decade) frequency range at each temperature, but as noted in the following, the same a_T data are found to correlate certain features of the dielectric

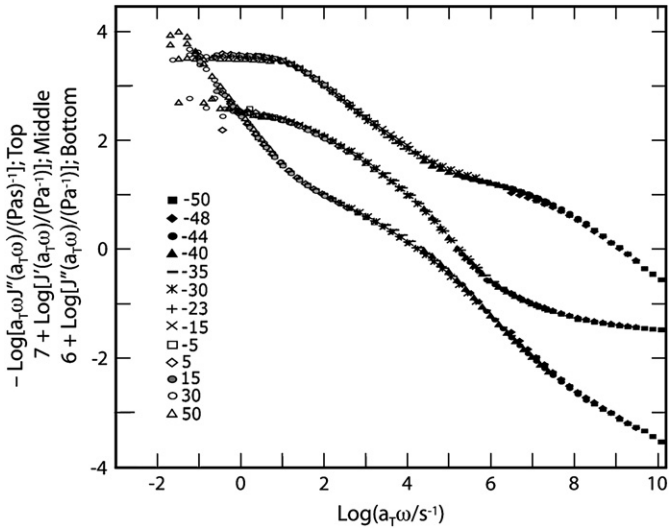

Fig. 1. Viscoelastic properties of GP5 superposed using the reduced frequency $a_T\omega$ (15 °C reference temperature) for the temperatures shown: $\log[1/a_T\omega J''(a_T\omega)]$, $7 + \log[J'(a_T\omega)]$ and $6 + \log[J''(a_T\omega)]$ from top to bottom.

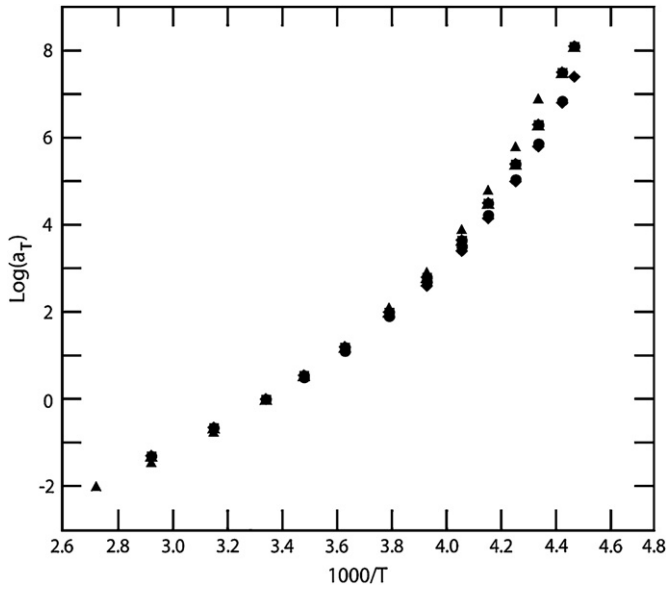

Fig. 2. The parameter $\log(a_T)$ vs $1000/(T/K)$ used to superpose the viscoelastic data shown in Figs. 1, and 3–5; unfilled circles, diamonds, triangles and squares and the filled versions of these in the same order are for GP5, GP1, GP3, GP4, PMM2a, PMM2d HL2 and HL3, respectively (symbol overlap obscures some of the symbols).

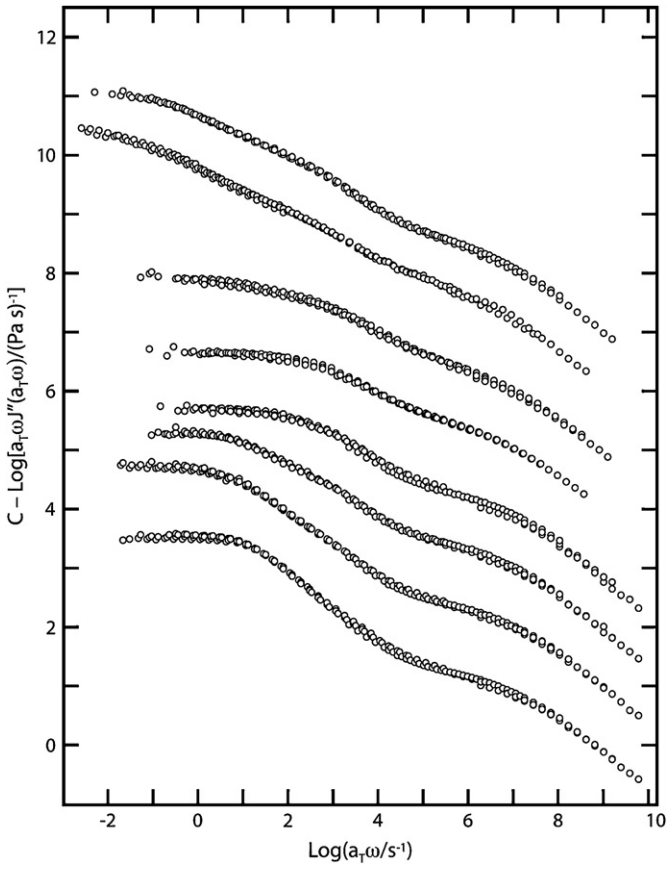

Fig. 3. The function $C + \log[1/a_T\omega J''(a_T\omega)]$ vs $\log(a_T\omega)$ from bottom to top for copolymers GP5 ($C = 0$), GP1 ($C = 1$), GP3 ($C = 2$) and GP4 ($C = 3$), macromonomer homopolymers PMM2a ($C = 4$) and PMM2d ($C = 5$), and brush-shaped polymers HL2 ($C = 6$) and HL3 ($C = 7$).

behavior over a wider range of frequency. The low frequency plateau in bilogarithmic plots of $a_T\omega J''(a_T\omega)$ as a function of $a_T\omega$ was used to estimated the viscosity η at the reference temperature, based on the limiting behavior of Eq. (2) as ω tends to zero, i.e., $[a_T\omega J''(a_T\omega)]^{-1}$ tends to $\eta(T_{ref})$ as $a_T\omega$ tends to zero, see Fig. 3; here, and in several following figures, the data have been separated along the ordinate by the addition of increments given in the figure caption. Values so deduced are included in Table 2, including an estimate for HL3 even though inspection of Fig. 2 suggests that the true limiting behavior may not have been attained for that sample, in which case the estimate for η would be too low. Bilogarithmic plots of $J'(a_T\omega)$ and $J''(a_T\omega) - 1/\omega\eta$ as functions of $a_T\omega$ for all of the samples studied are shown in Figs. 4 and 5, respectively (note that whereas the term $1/\omega\eta$ should read $1/(a_T\eta h_T)$ in general, with $h_T = a_T b_T$, the form given results if $b_T = 1$ as used here). In each, the data for sample GP5 are shown as a smoothed curve for the remaining samples, adjusted for superposition at the largest $a_T\omega$, a frequency range for which the effects of structural differences among the samples should be minimized.

Table 2
Characterization and viscosity

Series	λ	p	g	M_w/M_n	M_w/kDa	$\log(\eta/Pa.s)$
GP5	0.64	10	0.67	1.11	98	3.53
GP1	0.48	10	0.54	1.59	164	3.70
GP3	0.21	35	0.26	1.26	253	3.30
GP4	0.18	11	0.34	1.25	85	2.70
PMM2a	0.038	22	0.16	1.31	100	2.65
PMM2d	0.038	35	0.12	1.47	203	2.90
HL2	0.048	400	0.055	1.32	1430	4.30
HL3	0.024	400	0.031	1.30	2760	3.98

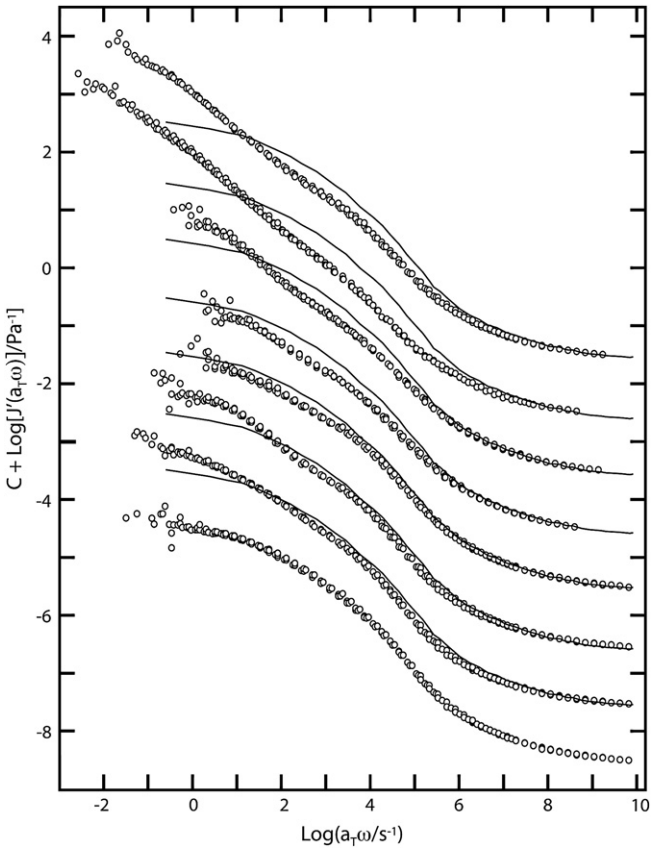

Fig. 4. The function $C + \log[J'(a_T\omega)]$ vs $\log(a_T\omega)$ with the values of C as in Fig. 3. The curves represent the data for GP5, slightly shifted to superpose the curve with the data for higher frequency to facilitate comparison with the response for the other samples.

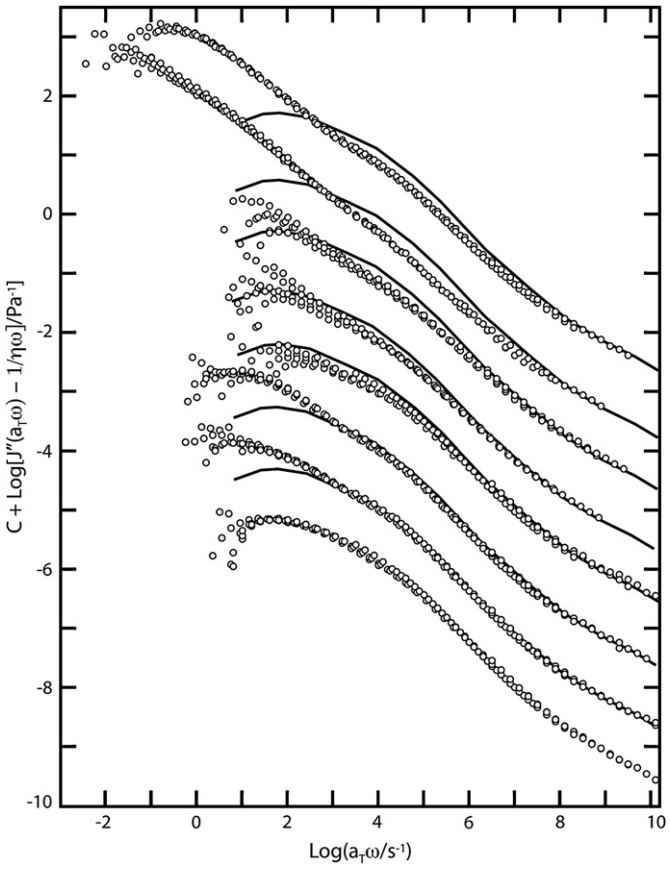

Fig. 5. The function $C + \log[J''(\omega) - 1/\omega\eta]$ vs $\log(a_T\omega)$ with the values of C as in Fig. 3. The curves represent the data for GP5, slightly shifted to superpose the curve with the data for higher frequency to facilitate comparison with the response for the other samples.

3.2. Dynamic dielectric properties

The data on $\varepsilon'(\omega)$ exhibit temperature-dependent plateaus at both lower and higher ranges of ω. That feature requires a temperature dependent $\Delta\varepsilon$, and the use of a factor $b_T^{(\varepsilon)} = \Delta\varepsilon(T)/\Delta\varepsilon(T_{\mathrm{ref}})$ in superposed plots of $\varepsilon'(\omega)$ and $\varepsilon''(\omega)$ as a function of frequency over a range of temperature; the simple expression $b_T^{(\varepsilon)} \approx (T_{\mathrm{ref}}/T)^{1/2}$ fitted the results and was used throughout; we are not aware of a theoretical justification for this empirical correlation, employed here as a convenient approximation within the precision of the data. Bilogarithmic plots of $\varepsilon'(a_T\omega)/b_T^{(\varepsilon)}$ and $\varepsilon''(a_T\omega)/b_T^{(\varepsilon)}$ as functions of $a_T\omega$ using the a_T obtained for the lower frequency response (i.e., for frequencies less than that for the upper bound of the principal peak, centered near $a_T\omega \approx 10^6\ \mathrm{s}^{-1}$) are given in Fig. 6 for sample GP5, for $T_{\mathrm{ref}} = 15\ ^\circ\mathrm{C}$, as with the viscoelastic data. The values of a_T were selected by imposing a fit starting with the data near the maximum value of $\varepsilon''(a_T\omega)/b_T^{(\varepsilon)}$, and as may be seen in Fig. 7, the a_T so obtained for all of dielectric data were essentially equal to those for the viscoelastic data for all of the samples studied (hence, no separate symbol was imposed to differentiate between the a_T used for the viscoelastic and dielectric functions). The data in Fig. 6 show a sharp increase in $\varepsilon'(a_T\omega)/b_T^{(\varepsilon)}$ with decreasing $a_T\omega$ at the lowest frequencies, with some loss of superposition, before the low frequency plateau in $\varepsilon'(a_T\omega)/b_T^{(\varepsilon)}$ is reached at slightly higher frequency. That low frequency upswing is attributed to electrode polarization [7], an instrumental artifact not of interest here. The region of the low frequency plateau in $\varepsilon'(a_T\omega)/b_T^{(\varepsilon)}$ is accompanied by behavior with $\varepsilon''(a_T\omega)/b_T^{(\varepsilon)} \propto (a_T\omega)^{-1}$, succeeded by a minimum in $\varepsilon'(a_T\omega)/b_T^{(\varepsilon)}$, followed by the principal peak in $\varepsilon''(a_T\omega)/b_T^{(\varepsilon)}$ at larger frequencies (the peak for $a_T\omega \approx 10^6\ \mathrm{s}^{-1}$). The $\varepsilon''(a_T\omega)/b_T^{(\varepsilon)} \propto (a_T\omega)^{-1}$ behavior is attributed to ionic conduction incurred by a small amount of an ionic impurity, and is of little interest except to note that $\varepsilon''(a_T\omega)/b_T^{(\varepsilon)}$ in the conduction and principal peak regimes scale with the same factor a_T, as is frequently observed with polymeric materials; though important in $\varepsilon''(a_T\omega)$ the conduction has no component in $\varepsilon'(a_T\omega)$ (similar to the importance of the viscosity on $J''(\omega)$, but not on $J'(\omega)$) [7]. The failure of the data to superpose on the

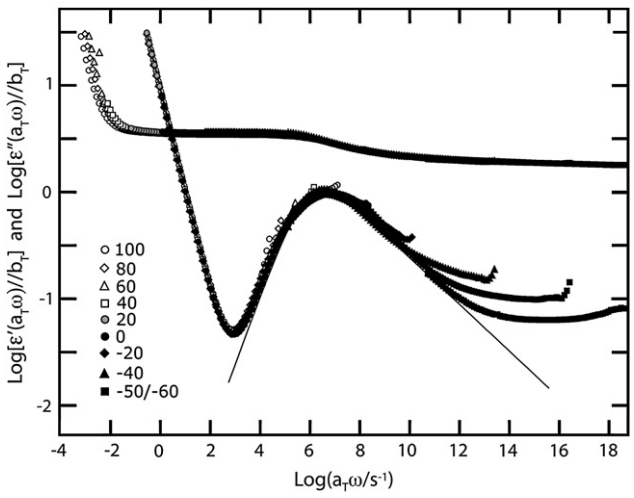

Fig. 6. Dielectric properties of GP5 superposed using the reduced frequency $a_T\omega$ (15 °C reference temperature) for the temperatures shown: $\log[\varepsilon'(a_T\omega)/b_T^{(\varepsilon)}]$ and $\log[\varepsilon''(a_T\omega)/b_T^{(\varepsilon)}]$ from top to bottom. The solid line represents the fit using Eq. (6) and the values $\alpha = \beta = 0.34$, as discussed in the text. (The data for −50 and 60 °C are not distinguished by symbol owing to overlap.)

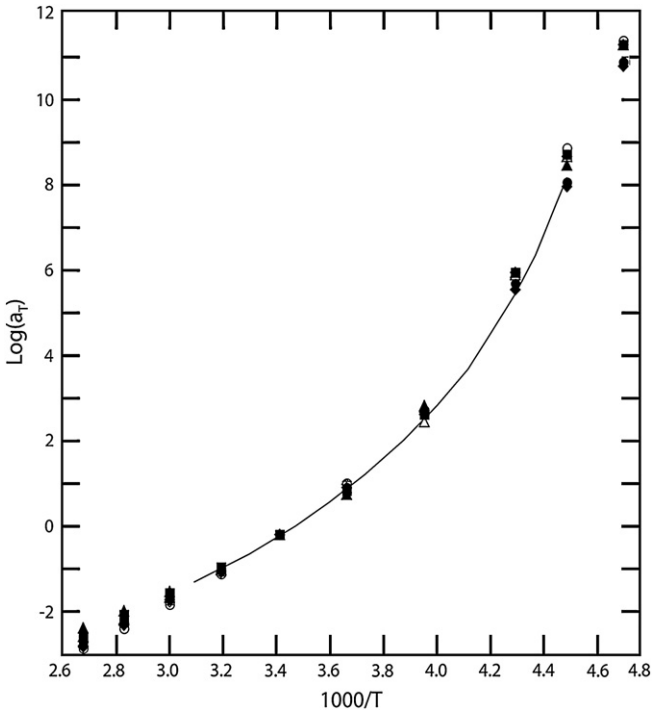

Fig. 7. The parameter $\log(a_T)$ vs $1000/(T/\mathrm{K})$ used to superpose the dielectric data shown in Figs. 6 and 8. The curve represents the viscoelastic a_T shown in Fig. 2, and the symbols are as in Fig. 2.

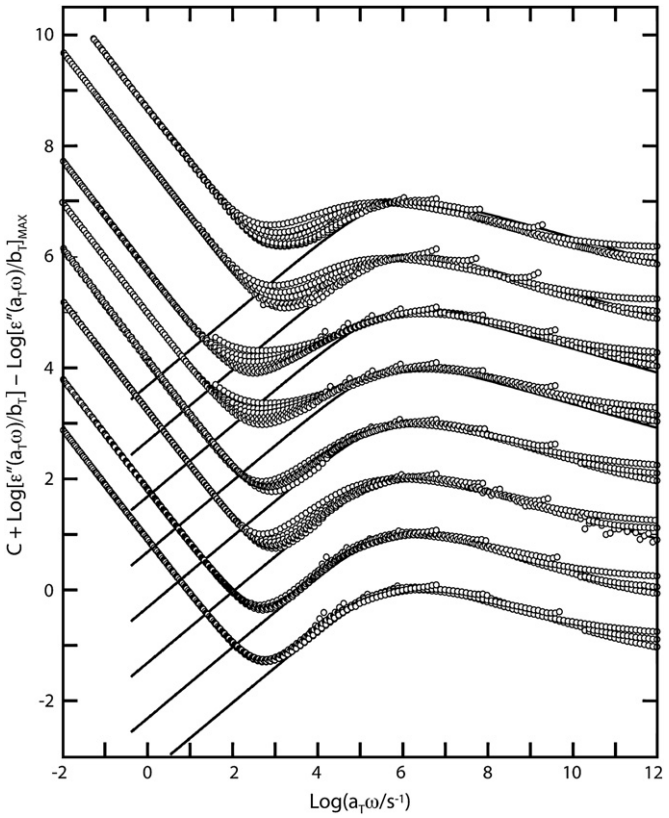

Fig. 8. The function $C+\log[\varepsilon''(a_T\omega)/b_T^{(\varepsilon)}]-\log[\varepsilon''(a_T\omega)/b_T^{(\varepsilon)}]_{\mathrm{MAX}}$ vs $\log(a_T\omega)$ with the values of C in Fig. 3; see the text for values of $[\varepsilon''(a_T\omega)/b_T^{(\varepsilon)}]_{\mathrm{MAX}}$. The curves represent the data for GP5, slightly shifted to superpose the curve with the data for higher frequency to facilitate comparison with the response for the other samples.

high-frequency side of the principal peak is a feature commonly observed with dielectric data, reflecting a change in the nature of the dielectrically active moiety at high frequencies, reflected in a changed dependence on temperature [7]. Although the high-frequency data can be superposed by use of separate $b_T^{(\varepsilon)}$ and $a_T^{(\varepsilon)}$ in that region that behavior is not investigated here. The principal peak in $\varepsilon''(a_T\omega)/b_T^{(\varepsilon)}$ is typical of that reported for p*n*BA [9], which was fitted by the empirical three-parameter Havriliak–Negami (HN) approximation which [7,10]

$$\left[\varepsilon''(\omega)-\varepsilon_{\mathrm{g}}\right]/\Delta\varepsilon \;=\; R(\omega\tau)^{-\beta/2}\,\sin(\beta\vartheta(\omega\tau)) \tag{6a}$$

$$R(x) \;=\; \left[1+x^{1-\alpha}\,\sin(\alpha\pi/2)\right]^2+\left[x^{1-\alpha}\,\cos(\alpha\pi/2)\right]^2 \tag{6b}$$

$$\tan[\vartheta(x)] \;=\; x^{1-\alpha}\,\cos(\alpha\pi/2)/\left[1+x^{1-\alpha}\,\sin(\alpha\pi/2)\right] \tag{6c}$$

where α, β and τ are parameters in the correlation; $\varepsilon''(\omega)$ has a maximum at frequency ω_{MAX}, such that $\tau\omega_{\mathrm{MAX}}$ depends on α and β. Although not used here, an explicit expression for $\tau\omega_{\mathrm{MAX}}$ is available [7,11]; the implicit expression for $\tau\omega_{\mathrm{MAX}}$ presented by HN contains an error. For $\omega\ll\omega_{\mathrm{MAX}}$ and $\omega\gg\omega_{\mathrm{MAX}}$ the HN function for $\varepsilon''(\omega)$ reduces to power laws with the exponents α and $\alpha\beta$, respectively. This function provides a reasonable fit to the central peak for sample GP5, using essentially the same parameters as those in Ref. [9], i.e., $\alpha=\beta=0.34$,with τ chosen to fit the peak frequency.

A bilogarithmic plot of $[\varepsilon''(a_T\omega)/b_T^{(\varepsilon)}]/[\varepsilon''(a_T\omega)/b_T^{(\varepsilon)}]_{\mathrm{MAX}}$ vs $a_T\omega$ for the data obtained here using the a_T in Fig. 7 is given in Fig. 8, along with curves for the Havriliak–Negami fit to the data on GP5 shown for comparison with each of the data sets; here, $[\varepsilon''(a_T\omega)/b_T^{(\varepsilon)}(\omega)]_{\mathrm{MAX}}$ is the value at the maximum of the principal peak centered between $a_T\omega\approx10^6$ and $10^7\ \mathrm{s}^{-1}$, with $\log[\varepsilon''(a_T\omega)/b_T^{(\varepsilon)}]_{\mathrm{MAX}}$ given by -0.55, -0.52, -0.50, -0.47, -0.50, -0.51, 0.13 and -0.66 for polymers GP5, GP1, GP3, GP4, PMM2a, PMM2d, HL2 and HL3, respectively. The data have been separated along the ordinate by the addition of increments given in the figure caption. A striking feature of these data, discussed further below, is the failure of the data to superpose for frequencies intermediate to regime with $\varepsilon''(a_T\omega)/b_T^{(\varepsilon)}\propto(a_T\omega)^{-1}$ and the principal peak, extending to the lower frequency side of the central peak for the samples with highest branch density. The corresponding data for $\varepsilon'(a_T\omega)/b_T^{(\varepsilon)}$ vs $a_T\omega$ are not included as the data for all of the samples were qualitatively similar to those shown in Fig. 6, with values of $\log[\varepsilon'(a_T\omega)/b_T^{(\varepsilon)}]$ in the low frequency plateau given by 0.57, 0.58, 0.64, 0.66, 0.68, 0.66, 1.22 and 0.50 for polymers GP5, GP1, GP3, GP4, PMM2a, PMM2d, HL2 and HL3, respectively. It may be noted that the variation of these tends to follow the variation in $\log[\varepsilon''(a_T\omega)/b_T^{(\varepsilon)}]_{\mathrm{MAX}}$ given above, such that $\log[\varepsilon'(a_T\omega)/b_T^{(\varepsilon)}]-\log[\varepsilon''(a_T\omega)/b_T^{(\varepsilon)}]_{\mathrm{MAX}}$ is a constant with ±20%.

4. Discussion

4.1. Viscoelastic properties

To the first-approximation, one can expect the viscosity of branched polymers to depend on the root-mean-square radius of gyration R_{G} and the mass per unit contour length M_{L} according to the expression [12]:

$$\eta \;=\; \eta_{\mathrm{LOC}}\tilde{X}\left\{1+\left(\tilde{X}/\tilde{X}_{\mathrm{c}}\right)^{4.8}\right\}^{1/2} \tag{7}$$

where $\tilde{X}=\pi N_{\mathrm{A}}\rho R_{\mathrm{G}}^2/M_{\mathrm{L}}$ for a melt with density ρ, with η_{LOC} a temperature-dependent local viscosity, proportional to a local or segmental friction factor ζ_{LOC}, $\tilde{X}_{\mathrm{c}}=\pi N_{\mathrm{A}}\rho M_{\mathrm{c}}\widehat{a}/3M_{\mathrm{L}}^2$ is about 100 for

a variety of flexible chain polymers [12]. In these expressions, $R_G^2 = g\hat{a}L/3 = g\hat{a}M/3M_L$ with persistence length $\hat{a}$, contour length $L = M/M_L$ of a linear chain of molecular weight M and g the ratio R_G of the branched polymer to its linear homologue of the same molecular weight. Eq. (7) is known to underestimate η if the branches are long, e.g., in excess of M_c for comb-shaped branched polymers, or longer than that for star-shaped branched chains [5,13,14].

The parameter M_L may be calculated as the ratio m_0/l of the molar mass m_0 of a repeat unit of contour length l; for vinyl polymers such as those of interest here l is independent of the substituents on the chain, and is convenient here to note that owing to this constancy, $\bar{X} \propto \rho g \mathrm{DP_w} \hat{a}/M_L$, where the weight-average degree of polymerization $\mathrm{DP_w}$ is used to account for molecular weight dispersity, and the critical degree of polymerization $\mathrm{DP_c}$ for the onset of entanglements for a (undiluted) linear polymer is given by $\bar{X}_c \approx \rho \mathrm{DP_c} \hat{a}/M_L$. Since analysis of data on the dependence of the intrinsic viscosity on molecular weight indicates that $\hat{a}/M_L$ is about the same for P*n*BuA and poly(ethyl acrylate), PEA [15], the published data on η as a function of $\mathrm{DP_w}$ and $\mathrm{DP_c}$ for PEA provide a convenient comparison with the data here on P*n*BuA, and will be introduced in the following. The simple expression

$$g \approx \lambda + \left[(3p-2)/p^2\right](1-\lambda)^{7/3} \tag{8}$$

for $g = (R_G^2)_{br}/(R_G^2)_{lin}$ provides a close representation of g for star and comb-shaped branched chains, with p the number of branches and λ the fraction of chain units in the backbone (e.g., tending to unity and zero as the chain adopts linear or star-shaped structures, respectively) [16]. It has been suggested that an equivalent expression with g replaced by the ratio $\hat{g} = (R_G^2)_{long}/(R_G^2)_{lin} = M_{long}/M$ be used to estimate η for randomly-branched chains, where $(R_G^2)_{long}$ and M_{long} are the mean-square radius of gyration and the molecular weight, respectively, of the longest linear sequence that exists in the branched structure [17]. In fact, $\hat{g}$ is 5–7% lower than g for most of the samples studied here, being about 28% smaller for the PMM series samples. The results for η versus $g\mathrm{DP_w}$ and $\hat{g}\mathrm{DP_w}$ are shown in Fig. 9, along with data on linear PEA and P*n*BuA samples (both corrected to constant η_{LOC}) [18,19]. As mentioned above, $\eta(15\,^\circ\mathrm{C})$ was determined as the value of $[a_T\omega J''(\omega)]^{-1}$ in the limit of small ω (see Fig. 3), and the products $g\mathrm{DP_w}$ or $\hat{g}\mathrm{DP_w}$ were determined using the data in Table 1 from Ref. [4].

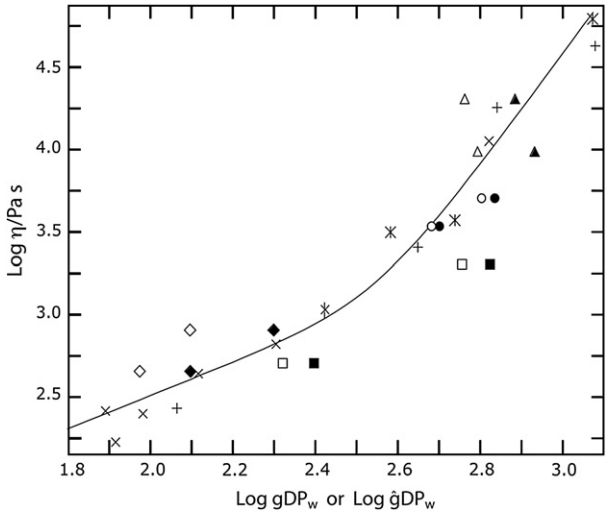

Fig. 9. $\log(\eta)$ vs $\log(g\mathrm{DP_w})$ (unfilled symbols) or $(\hat{g}\mathrm{DP_w})$ (filled symbols) for GP5 and GP1 (circles); GP4 and GP3 (squares); PMM2a and PMM2d (diamonds) and HL3 and HL2 (triangles). The entries for each pair are in the order of increasing η given in Table 2. Data from the literature for linear polymers are included for poly(ethyl acrylate) (×, Ref. [18], +, Ref. [19]) and poly(*n*-butyl acrylate) (✳, Ref. [19]). The solid curve is described in the text, and as mentioned in the text, the entry for HL3 may be too low.

The data in Fig. 9 on the P*n*BuA samples exhibit more scatter than would be anticipated from the quality of the viscoelastic data, suggesting that the presumed correlation is inadequate in some way. The dependence of $\hat{a}$ on the branch structure offers one possibility. An analysis of the intrinsic viscosity of comb-shaped polystyrenes gave such a dependence, with $\hat{a}/\hat{a}_{lin} \propto (M_L/M_{L,lin})^{\varepsilon}$, where $\varepsilon \approx 1.4$ for those polymers; M_L for the comb-shaped chain was computed to include the molar weight of the side chain, i.e., $M_L/M_{L,lin} = (1 + \mathrm{DP_{br}})$ [15]. This effect is most conveniently included by including a factor $(\hat{a}/\hat{a}_{lin})$ in the calculation of $(R_G^2)_{long}$ for use in $\hat{g}$ in an analysis of the dependence of η on $\hat{g}\mathrm{DP_w}$, and that has been done for the filled symbols in Fig. 9. In this treatment, the two lower DP brush-shaped polymers (series PMM) were treated as triblock copolymers, with end blocks comprising the "branches" attached to the terminal repeat units, and the central block comprising the remainder of the structure, with only the latter experiencing an enhanced $\hat{a}/\hat{a}_{lin}$. A published expression for R_G for a triblock copolymer without excluded volume effects was used [20]. The results in Fig. 9 suggest some improvement in the correlation, but significant deviations remain, particularly for the brush-shaped HL3; as noted above, the data on $[a_T\omega J''(\omega)]^{-1}$ in the limit of small ω suggest that the true limiting value may not have been reached for HL3, such that the value of η reported in Table 2 may be erroneously low. The behavior in Fig. 9 indicates that only the five highest molecular weight samples are in the entanglement regime (i.e., GP1,3,4,5 and HL2,3), and that the remaining three samples are below the entanglement condition (i.e., GP4 and PMM2a,d).

The data on $J'(\omega)$ in Fig. 4 show that $J'(a_T\omega)$ is essentially the same for samples GP1,3 and 5 for $a_T\omega > 100\ \mathrm{s}^{-1}$, but that $J'(a_T\omega)$ for GP1,3 becomes increasingly larger than that for GP5 for smaller $a_T\omega$. Further it may be seen that the smallest attainable $a_T\omega$ was not low enough to provide definitive values of J_S from the limiting value of $J'(\omega)$ at small ω; the values of $\log[J'(a_T\omega = 10^{-0.5})]$ for $\log[a_T\omega] = -0.5$ equal to −4.40, −4.10 and −4.14 for samples GP5,1 and 3 with λ equal to 0.64, 0.48 and 0.21, respectively. In the prior work the effects on J_s for the comb-branched polymer in the entanglement regime were interpreted in an approximate way by treating the branches as a diluent in calculating estimates for these quantities [1,13]. Thus, in that work, J_s for the entangled polymer was interpreted by the expression normally used for a flexible linear chain present at concentration c, with c replaced by the concentration $c_{bb} = \rho\lambda$ of the backbone chain to give

$$J_S \propto \frac{M_{ent}}{\rho\lambda^2 RT} \tag{9}$$

where M_{ent} is the entanglement molecular weight. It may be seen that the deviation between $J'(\omega)$ for samples GP1 and 3 from the data for GP5 increases with decreasing $a_T\omega$, as expected with this simple model. Accordingly, the estimates for $\log(J_S)$ for samples GP1 and GP3 would be expected to be larger than that for GP5 by 0.25 and 0.96, respectively. The estimates of $\log[J'(a_T\omega = 10^{-0.5})]$ quoted above give a similar increment for GP1, but a far smaller one for GP3, consistent with the indication from the shapes of the functions observed for these samples which suggest that the limiting behavior GP3 must lie at much smaller $a_T\omega$ than was experimentally accessible. As with the prior studies on brush-shaped polymers [1], it may be seen in Fig. 4 that the data on $J'(\omega)$ do not exhibit any tendency to approach a plateau at low ω, showing that J_S is strongly enhanced, consistent with the expectation with Eq. (9) and the small value of λ.

The features described in the preceding for $J'(\omega)$ are reflected in the behavior for $J''(\omega) - 1/\omega\eta$ shown in Fig. 5. The data for GP series tend to coincide at moderate to higher ω, as would be expected, with this coincidence moving to higher ω for the series PMM and

HL polymers with their high branch density (low λ), echoing the behavior reported for the brush-shaped polymers in Ref. [1].

4.2. Dielectric properties

To equivalence of a_T for the viscoelastic data on the temperature dependence of the dielectric data for $\varepsilon'(\omega)$ and the principal peak in $\varepsilon''(\omega)$ as well as the behavior at low ω indicates that the temperature dependence of these features of the dielectric response is controlled by the same segmental response that determines the temperature dependence of the viscoelastic response, as is usual [21]. The deviation from the reduced curve that occurs for the higher frequencies also duplicates behavior reported for p(*n*-BuA) and other polymers, leading to additional relaxation at high frequencies, and is not discussed further. The failure of the data to superpose for $a_T\omega$ near $10^3\ s^{-1}$ is discussed below. The principal peak, with a maximum $a_T\omega$ near $10^6\ s^{-1}$, is seen to occur in the range of $a_T\omega$ for which $J'(a_T\omega)$ and $J''(a_T\omega) - 1/\eta\omega$ are in the so-called transition from the short time (glassy) response to the terminal response [5,6]. This is the normal behavior for a dielectric α-relaxation [21]. As noted above, the behavior seen in Fig. 6 for GP5 is similar to that reported in the literature for linear p(*n*-BuA) [9], shown as the solid curve in Fig. 6, and the principal peak may be fitted by Eq. (6). This function has been included for comparison with each of the data sets in Fig. 8.

The superposition failure mentioned above is most evident in Fig. 8 for frequencies $a_T\omega$ near $10^3\ s^{-1}$ in the range of the $a_T\omega$ for the minimum $\varepsilon''(\omega)$ between the principal α-relaxation peak and the low frequency behavior with $\varepsilon''(\omega) \propto \omega^{-1}$, with the deviation becoming more apparent on the low ω side of the α-relaxation peak with decreasing λ. This superposition failure reflects a process with a different temperature dependence than that shared in common by the α-relaxation and the ionic conductivity seen in the low frequency behavior, as well as that seen in the viscoelastic response. Aside from effects inherent in the temperature dependence of the dynamic response on different time scales that may occur even for a noncrystalline homopolymer [5,6,22], superposition failure is frequently caused by some sort of physical heterogeneity in the sample, such as a crystalline component, phases differing in composition or blocks of repeating units differing in composition or stereostructure. Such behavior is often accompanied by a broadened glass transition; although no systematic study was done on all of the polymers examined here, no pronounced broadening was observed with the several examples tested. It may be noted that behavior similar to that seen here has been reported for polymers with side-chain groups that exhibit liquid-crystalline organization, with a so-called δ-relaxation at frequencies below or on the low ω side of the α-relaxation, with an early example featuring studies on a side-chain substituted polyacrylate [23]. In more recent studies, one, providing some historical review of the subject, included poly(methyl methacrylates) with each of four related, but different side-chain substituents, two of which formed a mesophase, and two of which did not [24], and another explored a poly(methyl acrylate) with a mesogenic sidegroup displaying a transition from nematic to smectic order with decreasing temperature [25]. The δ-relaxation was seen in these cases, being strong in the mesogenic samples, and weak in comparison with the α-relaxation for the nonmesogenic polymers in the isotropic state. The δ-relaxation was attributed to correlated motions along axis of the side-chain, with the temperature dependences of the α- and δ-relaxation being dissimilar. The frequency–temperature superposition failure observed in this study is attributed to a similar effect, with the δ-relaxation becoming stronger with increasing density of the side-chain substitution, indicating the effects of congestion at the branch node. A possibly related behavior has been reported in nuclear Overhauser effect (NOE) NMR relaxation studies of p*n*BA and related poly(*n*-alkyl acrylates), in which a response was noted at frequencies below those for the α-relaxation in dielectric measurements on the same materials [26]. The slow response was attributed to restricted mobility for relative motion of neighboring ^1H probed by NOE NMR, largely the ^1H on the CH_3– alkyl groups. That restriction was attributed to local poorly ordered domains, similar to those invoked in the preceding for the dielectric behavior observed here, even though the responses for the dielectric and NMR relaxations differ in origin. A somewhat similar notion of the effects of increasing length scale of intermolecular effects on the low frequency behavior of $\varepsilon''(\omega)$ was invoked in an approximate model designed particularly for behavior in the glassy state [27].

Inspection of Fig. 8 shows that the frequency range for which the frequency–temperature superposition fails is bounded by $10^2 < a_T\omega/s^{-1} < 10^5$, with the extent of the failure increasing with increasing branch density. It is likely that the feature extends to lower $a_T\omega$, but is not visible owing to the increasingly strong contributions with decreasing ω from the conduction band in that region. Comparison with Fig. 5 shows that this is the frequency range for which $J''(\omega) - 1/\omega\eta$ tends to a maximum for the brush-shaped copolymers, with that maximum pushed to still higher frequency for the high molecular weight brush-shaped homopolymers. Similarly, over the same frequency range, $J'(\omega)$ is approaching its maximum J_S for the comb-shaped copolymers, but is still increasing strongly with decreasing frequency for the brush-shaped homopolymers. This is the frequency range for which the viscoelastic response is making the transition from short-scale behavior, unaffected by chain entanglements, to the behavior dominated by longer-scale intermolecular entanglement effects. As a consequence, the effects resulting in the superposition failure in the dielectric response, attributed above to the correlated motion of the side chains, though slow, would likely occur on short length-scales, and not have an appreciable viscoelastic response in comparison with that for long length-scale intermolecular effects.

5. Conclusions

The principal features of $J'(\omega)$ and $J''(\omega)$ reported here are similar to those discussed in the prior work on brush-shaped poly(*n*-butyl acrylates) [1]. That work focused on the very high value of J_S for the brush-shaped chains without crosslinking and the corresponding high equilibrium compliance J_e (or low equilibrium modulus $G_e = 1/J_e$) for such chains when crosslinked. This is understood as an application of Eq. (9), which attributes the high values of J_S or J_e to a dilution effect arising from the side chains on the values of these that would otherwise arise from the backbone chain for J_S, or the backbone chain between crosslink loci for J_e. The analysis here of the viscosity η for the comb- and brush-shaped polymers indicates the need to account for an increase of the persistence length $\hat{a}$ with increasing density of the side chains, following the behavior discussed elsewhere on the basis of conformational properties at infinite dilution [15]. The dielectric loss $\varepsilon''(\omega)$ demonstrates a deviation from frequency–temperature superposition at a certain range of frequency, with the deviation increasing with increasing density of the side chains. The deviation occurs for a frequency range for which $J'(\omega)$ and $J''(\omega)$ are approaching their terminal response, but no corresponding deviation from frequency–temperature superposition is noted for these functions. The dielectric behavior in this region is attributed to a δ-relaxation at frequencies lower than the principal α-relaxation, similar to behavior reported for certain polymers with mesogenic side chains [23,24]. With the latter, the δ- and α-relaxation do not depend on temperature in the same way, and the δ-relaxation is strongly enhanced as the mesogenic side chains are ordered at lower temperature. The behavior noted here is attributed to a similar effect reflecting the effects of congestion at the branch node in the comb- and brush-shaped polymers.

Acknowledgements

This study was initiated as collaboration between the laboratories of KM and TP prior to the untimely death of the latter. The HL2 and HL3 samples were kindly provided by Hyung-il Lee of the KM laboratory. Financial support from the National Science Foundation (DMR 05-49353 and CBET 06-09087) is gratefully acknowledged, as well as support for SO from Kaneka Corp., Japan.

References

[1] Pakula T, Zhang Y, Matyjaszewski K, Lee H-I, Boerner H, Qin S, et al. Polymer 2006;47:7198–206.
[2] Tsarevsky NV, Matyjaszewski K. Chem Rev 2007;107:2270–99.
[3] Matyjaszewski K, Xia J. Chem Rev 2001;101:2921–90.
[4] Ohno S, Matyjaszewski K. J Polym Sci Part A Polym Chem 2006;44:5454–67.
[5] Berry GC. Polymer rheology: principles, techniques and applications. In: Brady JRF, editor. Comprehensive desk reference of polymer characterization and analysis. Washington, DC: American Chemical Society; 2003. p. 574–623.
[6] Ferry JD. Viscoelastic properties of polymers. 2nd ed. New York: John Wiley & Sons Inc; 1979.
[7] Schönhals A, Kremer F. Analysis of dielectric spectra. In: Kremer F, Schönhals A, editors. Broadband dielectric spectroscopy. Berlin: Springer-Verlag; 2003. p. 59–98.
[8] Nikonorova NA, Barmatov EB, Pebalk DA, Diaz-Calleja R. Vysokomol Soed Ser A B 2005;47:1498–506.
[9] Gomez Ribelles JL, Meseguer Duenas JM, Monleon Pradas M. J Appl Polym Sci 1989;38:1145–57.
[10] Havriliak S, Negami S. Polymer 1967;8:161–205. Appendix 206–210.
[11] Boersma A, Van Turnhout J, Wuebbenhorst M. Macromolecules 1998;31:7453–60.
[12] Berry GC. J Rheol 1996;40:1129–54.
[13] Roovers J, Graessley WW. Macromolecules 1981;14:766–73.
[14] Berry GC, Fox TG. Adv Polym Sci 1968;5:262–357.
[15] Berry GC. Inter J Polym Anal Character 2007;12:273–84.
[16] Berry GC. J Polym Sci Part B Polym Phys 1988;26:1137–42.
[17] Valles EM, Macosko CW. Macromolecules 1979;12:521–6.
[18] Andreozzi L, Castelvetro V, Faetti M, Giordano M, Zulli F. Macromolecules 2006;39:1880–9.
[19] Barlow AJ, Day M, Harrison G, Lamb J, Subramanian S. Proc Royal Soc London Ser A 1969;309:497–520.
[20] Sdranis YS, Kosmas MK. Macromolecules 1991;24:1341–51.
[21] Kremer F, Schönhals A. Broadband dielectric spectroscopy. Berlin: Springer-Verlag; 2003. p. 729.
[22] Plazek DJ. J Rheol (NY) 1996;40:987–1014.
[23] Zentel R, Strobl GR, Ringsdorf H. Macromolecules 1985;18:960–5.
[24] Schönhals A, Gessner U, Ruebner J. Macromol Chem Phys 1995;196:1671–85.
[25] Floudas G, Mierzwa M, Schönhals A. Phys Rev E 2003;67:031705.
[26] Gaborieau M, Graf R, Kahle S, Pakula T, Spiess HW. Macromolecules 2007;40:6249–56.
[27] Schoenhals A, Schlosser E. Colloid Polym Sci 1989;267:125–32.